Draft version March 9, 2010
Preprint typeset using LaTeX style emulateapj v. 11/10/09

UNSTABLE PLANETARY SYSTEMS EMERGING OUT OF GAS DISKS

Soko Matsumura[1], Edward W. Thommes[1,2], Sourav Chatterjee[1] and Frederic A. Rasio[1]

Draft version March 9, 2010

Abstract

The discovery of over 400 extrasolar planets allows us to statistically test our understanding of formation and dynamics of planetary systems via numerical simulations. Traditional N-body simulations of multiple-planet systems without gas disks have successfully reproduced the eccentricity (e) distribution of the observed systems, by assuming that the planetary systems are relatively closely packed when the gas disk dissipates, so that they become dynamically unstable within the stellar lifetime. However, such studies cannot explain the small semimajor axes a of extrasolar planetary systems, if planets are formed, as the standard planet formation theory suggests, beyond the ice line.

In this paper, we numerically study the evolution of three-planet systems in dissipating gas disks, and constrain the initial conditions that reproduce the observed a and e distributions simultaneously. We adopt the initial conditions that are motivated by the standard planet formation theory, and self-consistently simulate the disk evolution, and planet migration by using a hybrid N-body and 1D gas disk code. We also take account of eccentricity damping, and investigate the effect of saturation of corotation resonances on the evolution of planetary systems. We find that the a distribution is largely determined in a gas disk, while the e distribution is determined after the disk dissipation. We also find that there may be an optimum disk mass which leads to the observed $a - e$ distribution. Our simulations generate a larger fraction of planetary systems trapped in mean-motion resonances (MMRs) than the observations, indicating that the disk's perturbation to the planetary orbits may be important to explain the observed rate of MMRs. We also find much lower occurrence of planets on retrograde orbits than the current observations of close-in planets suggest.

Subject headings: methods: numerical, n-body simulations, planetary systems: protoplanetary disks, formation, planets and satellites: formation, general

1. INTRODUCTION

Out of over 360 planetary systems discovered so far, about 12.4% are known to be multiplanet systems (http://exoplanet.eu/). Also, recent observations have started revealing that many of the detected planets are accompanied by a planet on a further orbit (e.g. Wittenmyer et al. 2007; Wright et al. 2007). It will become increasingly more important to understand the formation and evolution of multiplanet systems, which can explain the observed properties of extrasolar planetary systems.

Recent numerical N-body simulations of planetary systems *without* a gas disk demonstrated that dynamical instabilities occurring in the multiplanet systems, which are characterized by orbital crossings, collisions, and ejections of planets, could increase planetary eccentricities (e) efficiently (e.g., Rasio et al. 1996; Weidenschilling & Marzari 1996). These studies successfully reproduced the observed eccentricity distribution of extrasolar planets (Ford & Rasio 2008; Chatterjee et al. 2008; Jurić & Tremaine 2008, from here on C08, and JT08, respectively.)

Such N-body simulations also suggest that the planet–planet interactions alone cannot explain small semimajor axes (a) of the observed planets, *if* giant planets are formed beyond the ice line as expected from the standard planet formation theory. More specifically, starting with giant planet systems beyond 3 AU, C08 found that it is difficult to scatter planets within ~ 1 AU. This is because planet–planet interactions are not particularly efficient in shrinking the planetary orbits.

The disk–planet interactions, on the other hand, are known to decrease semi-major axes of planets efficiently (Ward 1997). The overall effect of such interactions on the orbital eccentricity is highly uncertain, and depends on a detailed disk structure, as well as planetary masses. Generally, disk–planet interactions lead to eccentricity damping, but for planets massive enough to open a clean gap in the disk, eccentricity can increase rapidly depending on the level of saturation of corotation resonances (Goldreich & Sari 2003; Moorhead & Adams 2008). However, hydrodynamic simulations show that the disk–planet interactions typically lead to $e < 0.2$ (e.g., D'Angelo et al. 2006).

The time to dynamical instability scales with the distance between planets (e.g., C08). Thus, all the N-body studies on planet–planet scattering assume initially dynamically active planetary systems (i.e., distance between planets being less than about a few Hill radii). However, with the aid of a gas disk, planets which would not easily reach dynamical instability could experience strong interactions. For example, when planets are embedded in the inner cavity of a disk, the surrounding disk would push the outer planet closer to the inner one, triggering the dynamical instability (e.g., Adams & Laughlin 2003; Moorhead & Adams 2005). The orbital eccentricity can also be increased if planets are trapped in mean motion resonances (MMRs) during such a convergent migration (e.g., Snellgrove et al. 2001; Lee & Peale 2002).

[1] Department of Physics and Astronomy, Northwestern University, Evanston, IL 60208, USA
[2] University of Guelph, Guelph, ON, Canada

Alternatively, when a gas disk annulus is left between planets, the eccentricities of planets could still increase by repeated resonance crossings due to divergent migration (Chiang et al. 2002). Thus, whether the combined effects of disk–planet and planet–planet interactions would lead to eccentricity excitation, or damping should be studied carefully. One of the goals of our study is to verify the initial assumptions of N-body studies (i.e., planets are on nearly circular, and coplanar orbits when the gas disk is around), and figure out whether the eccentricity distribution is largely determined before, or after the disk dissipation.

In this paper, we numerically study the evolution of three-planet systems in a dissipating gas disk, and constrain the "initial" conditions of planetary systems which can reproduce the a and e distributions simultaneously. We calculate the disk–planet interactions directly so that the disk and planetary orbits evolve self-consistently. Also, we take account of the effect of saturation of corotation resonances on eccentricity damping. We introduce the numerical methods in Section 2, and the initial conditions in Section 3. In Section 4, we show that the observed $a-e$ scattered plot can be reproduced well for a reasonable range of disk masses. We also discuss the mass distribution, and mean-motion resonances for representative cases. Finally in Section 5, we compare this work with some recent observations, and summarize our results.

2. NUMERICAL METHODS AND INITIAL CONDITIONS

To simulate multiplanet systems in gas disks, we use a hybrid code which combines the symplectic N-body integrator SyMBA (Duncan et al. 1998) with a one-dimensional gas disk evolution code (Thommes 2005). SyMBA utilizes a variant of the so-called mixed-variable symplectic (MVS) method (Wisdom & Holman 1991), which treats the interaction between planets as a perturbation to the Keplerian motion around the central star, and handles close encounters between bodies with a force-splitting scheme which has the properties of an adaptive timestep (Duncan et al. 1998). When the bodies are well-separated, SyMBA has the speed of the MVS method, while during the close encounters, the timestep for the relevant bodies is recursively subdivided.

On the other hand, the gaseous disk evolves both viscously and via gravitational interaction with planets, according to a general Navier-Stokes equation. Following the standard prescription by Lin & Papaloizou (1986), the gas disk is divided into radial bins, which represent disk annuli with azimuthally and vertically averaged disk properties like surface mass density, temperature, and viscosity. Viscous evolution of the disk is calculated by using the standard alpha viscosity prescription (Shakura & Sunyaev 1973), while the disk–planet interactions modify the disk evolution via the torque density formulated in Ward (1997) (see also Menou & Goodman 2004). The calculated torque density is used in turn to determine the migration rates of planets.

In our simulations, a disk stretches from 0.02 to 100 AU, and the orbital evolution of planets is followed down to 0.02 AU. The timestep of simulations is typically 0.05 yr, which ensures a reasonable orbital resolution down to ~ 0.2 AU.

2.1. *Gas Accretion onto a Planet*

The above code follows the evolution of planetary systems as planets gravitationally interact with each other, migrate, and open gaps in the disk. However, planets are also expected to clear the gas annuli between them as they grow by accreting gas from the surrounding disk.

Once a planet becomes massive enough to open a gap in the disk, the gas accretion rate is controlled by how quickly the disk can supply gas to the planet, rather than how quickly the planet can accrete gas (Bryden et al. 2000; Tanigawa & Watanabe 2002). Since all the planets in our simulations are more massive than the Neptune, they are expected to have circumplanetary disks, from which they accrete. Although our code does not resolve such disks, we can mimic the accretion effect by adopting the results of hydro simulations. Tanigawa & Watanabe (2002) showed that, without a gap-opening effect, a planet accretes gas within a few Hill radii on the following timescale.

$$\tau_{subdisk} = 30.76 \text{ yr } \left(\frac{M_p}{M_J}\right)^{-1/3} \left(\frac{\Sigma(r)}{1.7\times10^3 \text{ g cm}^{-2}}\right)^{-1} \quad (1)$$

Here, M is mass, and Σ is the surface mass density. The subscripts p, and J represent the planet, and Jupiter, respectively. Due to the gap-opening effect, the true accretion timescale is likely longer than the above estimate (e.g. D'Angelo et al. 2003). However, since our code handles a gap-opening due to disk-planet interactions separately, we adopt the above accretion timescale for all of our planets.

2.2. *Eccentricity Evolution*

For simplicity, we focus on eccentricity evolution due to the first-order resonances. Also, to evaluate the effects of eccentricity excitation due to planet–planet interactions, we neglect the e excitation due to disk–planet interactions.

When a planet is too small to open clean gaps, the eccentricity evolution is dominated by co-orbital Lindblad resonances which damp eccentricity (e.g. Artymowicz 1993). In such a case, the eccentricity damping timescale can be expressed as follows (e.g. Kominami & Ida 2004).

$$\tau_{edamp} = -\frac{e_p}{\dot{e_p}} = \left(\frac{h_p}{r_p}\right)^4 \left(\frac{M_*^2}{M_p\bar{\Sigma}_p r_p^2}\right) \Omega(r_p)^{-1} \quad (2)$$

Here, h is the pressure scale height, r is the orbital radius, and Ω is the orbital frequency. The subscript $*$ denotes the star. Note that the equation is evaluated at the location of a planet. Also, for the disk's surface mass density, we take the average of peri-center, semi-major axis, and apo-center of a planetary orbit.

On the other hand, when a planet becomes large enough to open a clean gap, the effect of co-orbital Lindblad resonances diminishes, and the competing effects of e excitation due to external Lindblad resonances and e damping due to corotation resonances become significant (Goldreich & Tremaine 1980). In such a case, the eccentricity damping can be written as follows (Goldreich & Sari 2003):

$$\tau_{edamp} = -\frac{e_p}{\dot{e_p}} = \frac{1}{K_e}\left(\frac{w}{r}\right)^4 \left(\frac{M_*^2}{M_p\Sigma r^2}\right) \Omega^{-1} \quad (3)$$

where $w = r(3\pi\alpha)^{-1/3}(r/h)^{2/3}(M_p/M_*)^{2/3}$ is a gap width which is determined by balancing the gap-opening tidal torque from the principal Lindblad resonances with the gap-closing viscous torque, and α is the standard viscosity parameter by Shakura & Sunyaev (1973). The above equation is evaluated at the gap edges, where the contribution from the resonances is the largest. The damping efficiency is governed by K_e, which is defined as below by following the approach of Goldreich & Sari (2003).

$$K_e = [1.046\, F(p) - 1]\,. \tag{4}$$

In this equation, $F(p)$ is the saturation function of corotation torques that is numerically evaluated by Ogilvie & Lubow (2002) and interpolated by Goldreich & Sari (2003) as

$$F(p) \simeq \frac{\left(1 + 0.65\, p^3\right)^{5/6}}{(1 + 1.022\, p^2)^2} \tag{5}$$

$$p \sim \left(\frac{r}{h}\right)^{2/9} (\frac{M_*}{M_p})^{1/9} \frac{e_p}{\alpha^{1/9}}. \tag{6}$$

For $K_e = 0.046$ (and hence $F(p) = 1$), the corotation torques are unsaturated, and fully contribute to the eccentricity damping, while for the other extreme $K_e = 0$, the effect of corotation torques are negligible, and there is no damping. Negative values of K_e corresponds to e excitation, but we don't take account of the effect here. Note, however, that hydrodynamic simulations show that the disk–planet interactions typically lead to $e < 0.2$ (e.g. D'Angelo et al. 2006), and therefore may not be able to explain planets with high eccentricities.

2.3. *Disk Dissipation Timescale*

C08 suggested that the dynamical instability occurs more frequently as the disk mass decreases. Generally, the lifetime of gas disks is estimated to be $1 - 10$ Myr (e.g. Hillenbrand 2005; Sicilia-Aguilar et al. 2006), but the mechanism of the final dispersal of disks is not well-understood.

Observations suggest that such a timescale is rather short, $\sim 10^5 - 10^6$ yr (e.g. Simon & Prato 1995; Currie et al. 2009). Since the viscous accretion timescale of a disk is longer than this, currently the most promising mechanism to explain the rapid dispersal of disks is photoevaporation, which can remove a disk within $10^5 - 10^6$ yr in favorable cases (Matsuyama et al. 2003; Alexander et al. 2006). Here, we simply treat the gas disk dissipation time as a parameter, and assume that the entire disk is removed exponentially once τ_{GD} is reached. In a Jupiter-mass disk, this disk removal timescale is about 10^5 yr.

3. INITIAL CONDITIONS

We study evolution of three-planet systems in a gas disk by changing various parameters. Specifically, we study five different disk masses with 200 planetary systems, by changing gas dissipation time τ_{GD} between $2 - 4$ Myr. We run each set of runs with and without the effect of saturation of corotation resonances. Our initial conditions are summarized in Table 1.

We focus on three-planet systems, and define their initial properties following C08. We determine the planetary masses by adopting a simplified core accretion scenario. Specifically, we sample planetary core masses randomly from a distribution over $1 - 100\, M_E$ (where M_E is the Earth mass) uniform in $M_{core}^{1/5}$, and assume that each core accretes all gas within the "feeding zone" that is extending over $\Delta = 8R_{hill,\,core}$, and centered on the core:

$$M_p = 2\pi a \Delta \Sigma + M_{core}.$$

Here, the core's Hill radius is defined as $R_{hill,\,core} = (M_{core}/(3M_*))^{1/3}a$. The size of the feeding zones is a typical distance between planetary embryos (Kokubo & Ida 2002).

As in C08, the semimajor axes are chosen so that the distance between planets is scaled with $K = 4.4$ times the Hill radius of the i-th planet:

$$a_{i+1} - a_i = K\, R_{hill,i},$$

with $a_1 = 3$AU. We fix the initial semimajor axis of the innermost planet following the common assumption that giant planets form beyond the "ice line", where the solid density is higher due to the condensation of icy and/or carbonaceous material (Lewis 1974; Lodders 2004). From this prescription, we obtain planets with mass ranging over $0.4 - 4\, M_J$, between 3 to 6.5 AU.

We make two independent sets of 100 three-planet systems. Since typical planetary eccentricities and inclinations just after planet formation are not known, we use two different ranges of initial e and i. For one of the sets (marked with $d1$ in Table 1), we choose initially moderate e and i, which are randomly drawn from a uniform distribution in the range of $e = 0 - 0.1$, and from a distribution uniform in $\cos i$ over the range of $i = 0 - 10$ deg, respectively. For the latter set (marked with $d2$ in Table 1), on the other hand, we choose initially small e and i over the range of $e = 0 - 0.05$, and $i = 0 - 0.03$ deg, respectively. The former set is identical to *Mass distribution 3* in C08. In both sets, phase angles are randomly chosen from a uniform distribution over $0 - 360$ deg. Also, gas disk dissipation time τ_{GD} is chosen randomly between $2 - 4$ Myr for each three-planet system.

Since our planets are nearly fully grown, we use evolved gas disks as the initial gas disks, instead of using the primordial ones. Each initial disk is generated by evolving the minimum mass solar nebula (MMSN)-type disk with $\Sigma = 10^3(a/AU)^{-3/2}\, g\, cm^{-2}$ for 5, 6, 7, 8, and 9 Myr without planets, under the disk's viscosity $\alpha = 5 \times 10^{-3}$. This corresponds to five different initial disk masses in the range of $\sim 0.3 - 1.6 M_J$. All disks are stretching from 0.02 to 100 AU.

These initial conditions are summarized in Table 1.

4. RESULTS

In Sections 4.1 and 4.2, we focus on the results of sets with initially moderate e and i (i.e., sets denoted by $d1$, see Table 1). Without a gas disk, C08 showed that N-body simulations of this type of three-planet systems reproduce the observed e distribution of exoplanets very well. On the other hand, by assuming that planets are formed beyond the ice-line (~ 3 AU), their simulations showed that it is difficult to scatter planets within ~ 1 AU. In Section 4.1, we discuss the effects of the initial

TABLE 1
Initial Disk Conditions

Set No.	τ_{disk}[Myr]	$M_{disk}[M_J]$	Distribution	K_e
t5d1	5	1.6	1	0.046
t6d1	6	1.1	1	0.046
t7d1	7	0.71	1	0.046
t8d1	8	0.47	1	0.046
t9d1	9	0.32	1	0.046
t5d1cr	5	1.6	1	CR
t6d1cr	6	1.1	1	CR
t7d1cr	7	0.71	1	CR
t8d1cr	8	0.47	1	CR
t9d1cr	9	0.32	1	CR
t5d2	5	1.6	2	0.046
t6d2	6	1.1	2	0.046
t7d2	7	0.71	2	0.046
t8d2	8	0.47	2	0.046
t9d2	9	0.32	2	0.046
t5d2cr	5	1.6	2	CR
t6d2cr	6	1.1	2	CR
t7d2cr	7	0.71	2	CR
t8d2cr	8	0.47	2	CR
t9d2cr	9	0.32	2	CR

Note. — Initial conditions for each set of 100 runs. Column 1 shows names of sets, where $t(5-9)$ indicates the age of initial disks, $d1$ and $d2$ represent two different distributions of 100 three-planet systems ($d1$ has larger initial e and i compared to $d2$, see Section 3), and cr for sets of runs taking account of saturation of corotation resonances. Column 2 shows the age of initial disks, which is obtained by evolving a MMSN-type disk under $\alpha = 5 \times 10^{-3}$. Column 3 lists the corresponding initial disk mass. Column 4 shows two different distributions of three-planet systems. Column 5 shows the eccentricity damping factor K_e, where 0.046 is full damping, and CR means that the saturation of corotation resonances is taken into account (see Section 2.2).

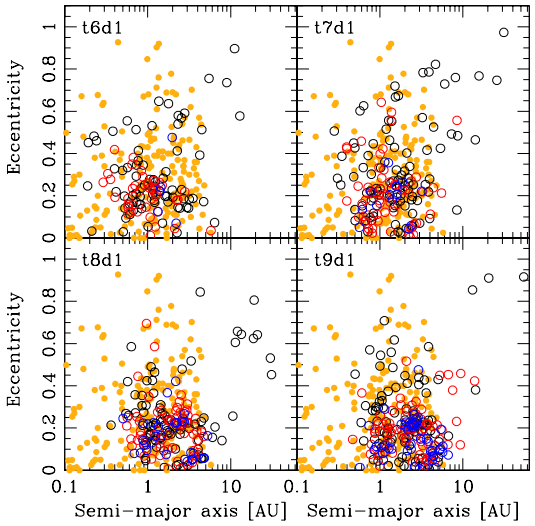

Fig. 1.— The final $a-e$ scattered plot for $t6d1-t9d1$. Black, red, and blue circles indicate the innermost, middle, and outermost planet, respectively. Orange solid circles are the observed exosolar planets. The 2D K-S tests for the observed and simulated distributions show that the null hypothesis cannot be rejected for $t6d1$ and $t7d1$.

disk mass on the $a-e$ distribution, while in Section 4.2, we study the effects of the saturation of corotation resonances. In Section 4.3, we investigate the corresponding results for initially small e and i. We discuss typical evolution cases in Section 4.4, and mass distribution in Section 4.5. Finally in Section 4.6, we study the mean motion resonances seen in our simulations.

4.1. *Effect of the initial disk mass*

First, we investigate the effects of initial disk masses on final distribution of a and e by neglecting the effects of saturation of corotation resonances (i.e., $t5d1-t9d1$). The $a-e$ scattered plots of planets after 100 Myr for $t6d1-t9d1$ are plotted in Fig. 1. Also plotted is the observed $a-e$ distribution. As expected, more massive disks have more planets with smaller semi-major axes, due to efficient planet migration.

The overall trend of the $a-e$ scattered plot is reproduced fairly well, especially for $t6d1$ and $t7d1$. We can quantify this by using the Kolmogorov-Smirnov (K-S) test. We perform the K-S tests against the null hypothesis that two arbitrary distributions are drawn from the same underlying distribution, and quote the significance level probabilities in Table 3. We choose to reject the null hypothesis for $P < 0.1$. To compare the observed and simulated distributions, we select planets between 0.2 and 6 AU with mass ranging over $0.3-4M_J$. The lower limit of semi-major axis comes from the resolution limit of our simulations (see Section 2), while the upper limit is motivated by the current maximum orbital radius of a planet detected by radial-velocity observations. Our two dimensional K-S tests indeed show that we cannot reject the null hypothesis of the observed and simulated distributions for $t6d1$ and $t7d1$. The agreement with the observed distribution becomes worse for more, or less massive disk cases ($t5d1$, $t8d1$, and $t9d1$). Thus, our results indicate that there may be an optimum disk mass to reproduce the observed $a-e$ distribution.

Now we look into the a and e distributions separately. Fig. 2 compares the observed and simulated a and e distributions at 100 Myr for $t6d1$, $t7d1$, and $t8d1$. For a distribution, the K-S test shows that we cannot reject the null hypothesis for $t6d1$ and $t7d1$ at 100 Myr, while for $t8d1$, the observed and simulated semi-major axis distributions are significantly different from each other. Thus, our results indicate that a disk mass less than $\sim 0.5M_J$ does not lead to significant planet migration. Efficient planet migration requires that an outer disk mass is comparable to, or larger than, the planetary mass (Ivanov et al. 1999). Since the mass range of our planets is $0.4-4M_J$, it is expected that lower disk mass cases have little planetary migration.

For e distribution, on the other hand, the K-S test shows that the null hypothesis cannot be rejected for $t7d1$ at 100 Myr. The distributions of $t8d1$ and $t9d1$ are dominated by planets with relatively small eccentricities ($e \lesssim 0.3$), indicating that these cases are more dynamically stable compared to $t7d1$. On the other hand, $t6d1$ has a deficit of planets with $e \lesssim 0.1$ and an overabundance of planets with $e \sim 0.2$. A similar deficit of planets with low eccentricities is reported by JT08 for disk-less cases.

Now, we compare the corresponding $a-e$ distributions at the disk dissipation time τ_{GD} with the observed distribution, to highlight the evolution of planetary systems while a gas disk is around. The 2D K-S tests reject the null hypothesis with the observed distribution for all of these sets ($t5d1-t9d1$) at τ_{GD}. This results indicate that planet–planet interactions *after* the gas disk dissipation

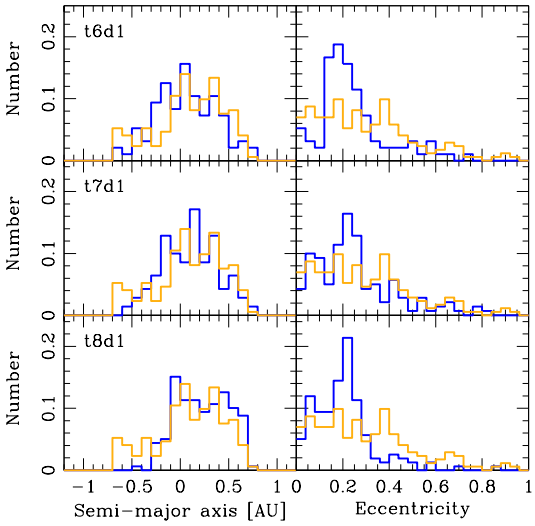

FIG. 2.— Left: Final a distributions for $t6d1$, $t7d1$, and $t8d1$ (blue histograms), compared with the observed distribution (orange histograms). Right: Corresponding e distributions. From the 1D K-S tests, the null hypothesis of the observed and simulated a distributions cannot be rejected for $t6d1$ and $t7d1$. Similarly, the null hypothesis for the e distributions cannot be rejected for $t7d1$.

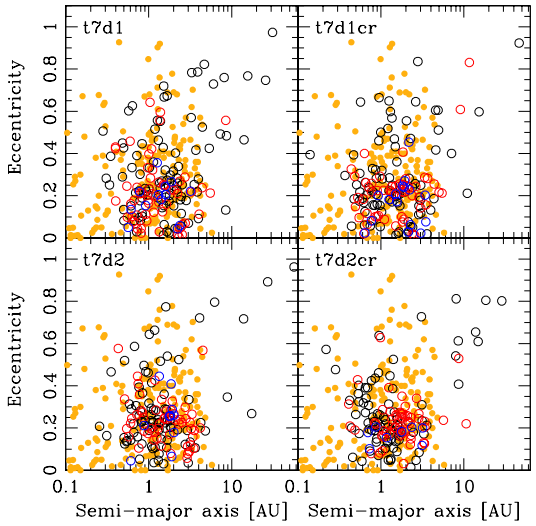

FIG. 3.— The final $a-e$ scattered plot for t7 cases. Upper panels have moderate initial e and i, while bottom panels have small initial e and i. Left panels don't take account of the effect of saturation of corotation resonances, while right panels do.

must have played a significant role in determining the final $a-e$ distribution. The 1D K-S tests support this statement. For the a distribution, the null hypothesis is rejected for all the sets but $t7d1$ at τ_{GD}, while for the e distribution, the null hypothesis is rejected for all five sets at τ_{GD}.

Overall, our results imply that the a distribution is largely determined while a gas disk is around, since the semi-major axis distribution does not change dramatically between τ_{GD} and 100 Myr. The e distribution is largely determined by planet–planet interactions after the disk dissipates, because the orbital eccentricities generally stay low while a gas disk is around. Thus, we find that the initial assumption of nearly circular orbits in the previous N-body studies is reasonable.

4.2. *Effect of the saturation of corotation resonances*

Next, we repeat the same set of simulations by taking account of the saturation of corotation resonances (i.e., $t5d1cr - t9d1cr$). The overall results turn out to be very similar to $t5d1 - t9d1$. In fact, as it can be seen from Table 3, the 2D K-S tests against the observed and final $a-e$ scattered plots show that the null hypothesis cannot be rejected for $t6d1cr$, and $t7d1cr$. The 1D K-S tests for a and e support this result. Furthermore, as in Table 2, the rates of ejections, collisions, and mergers are comparable for the cases with and without the saturation of corotation resonances, both before and after τ_{GD}. Since we don't take account of the e excitation due to the disk–planet interactions, the inclusion of the saturation of corotation resonances only prolongs the e damping time in our simulations. The fact that such effects do not dramatically change the final $a-e$ distribution implies that the eccentricity damping without the saturation of corotation resonances is as inefficient as that with saturation for the range of disk masses we use.

4.3. *Effect of initial e and i*

We also study the evolution of three-planet systems with initially small e and i (sets denoted with $d2$, see Table 1). The overall results are similar to the cases with moderate e and i, for both with and without the saturation of corotation resonances.

For cases *without* the saturation of corotation resonances ($t5d2 - t9d2$), the 2D K-S tests against the observed and final distributions show that the null hypothesis cannot be rejected for $t6d2$ and $t7d2$. On the other hand, for cases *with* the saturation of corotation resonances ($t5d2cr - t9d2cr$), the corresponding tests show that the null hypothesis cannot be rejected for $t7d2cr$ and $t8d2cr$. Thus, again, there seems to be an optimum disk mass to reproduce the $a-e$ distribution.

One significant difference for having initially small or moderate e and i values is the rate of mergers. When initial systems are closer to coplanar, the merger rates tend to be higher. By comparing $t5d1-t9d1$ with $t5d2-t9d2$, we find that the merger rates before τ_{GD} are $\sim 1.5-3$ times higher in $t5d2 - t9d2$, while the merger rates after τ_{GD} are comparable. Similarly, the comparison of $t5d1cr - t9d1cr$ with $t5d2cr - t9d2cr$ shows that the merger rates before τ_{GD} are $\sim 1.5-5$ times higher in the latter sets. We find that most of these mergers occur immediately after the start of the simulations, within 10^4 yr. Ford et al. (2001) studied the dynamical evolution of equal-mass two-planet systems, and found that mergers tend to produce low eccentricity ($e < 0.1$) planets. However, in our simulations, we do not find any statistically significant change in the fraction of low e planets between $d1$ and $d2$ cases.

Fig. 3 summarizes the $a-e$ scattered plots for $t7d1$, $t7d1cr$, $t7d2$, and $t7d2cr$ at 100 Myr. In all cases, the null hypothesis for the observed and simulated distributions cannot be rejected for $0.2\,\mathrm{AU} \leq a \leq 6\,\mathrm{AU}$.

4.4. *Various Evolution Cases*

Table 2 summarizes the dynamical outcomes of our simulations, and lists the rates of ejection out of the system, collision with the central star, and merger between

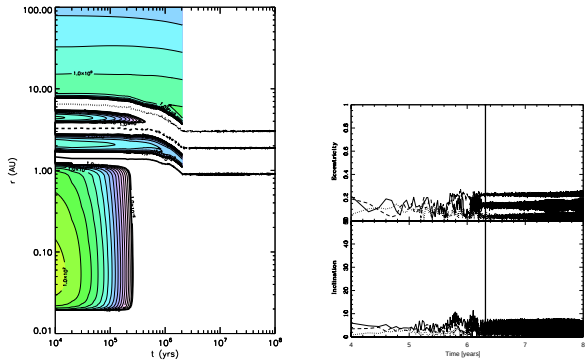

FIG. 4.— Evolution of a three-planet system. Left: Semi-major axis evolution of three planets. Colored contours show the surface mass density of a gas disk. The vertical truncation of the surface mass density corresponds to τ_{GD}. Right: Corresponding e and i evolution. The vertical line indicates τ_{GD}. No instability occurs for 10^8 yr.

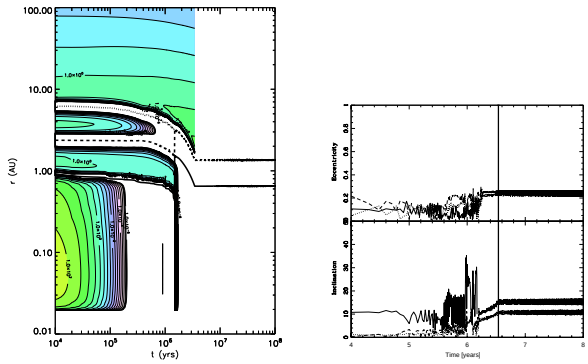

FIG. 5.— Evolution of a three-planet system similar to Fig. 4. Left: Semi-major axis evolution of three planets. Right: Corresponding e and i evolution. Dynamical instability before τ_{GD} leads to an ejection of a planet out of the system.

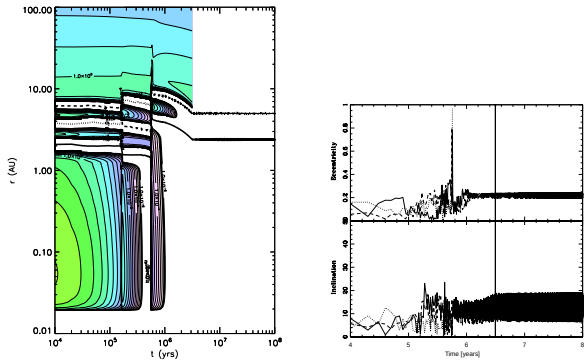

FIG. 6.— Evolution of a three-planet system similar to Fig. 4. Left: Semi-major axis evolution of three planets. Right: Corresponding e and i evolution. Dynamical instability before τ_{GD} leads to a collision of a planet with the central star.

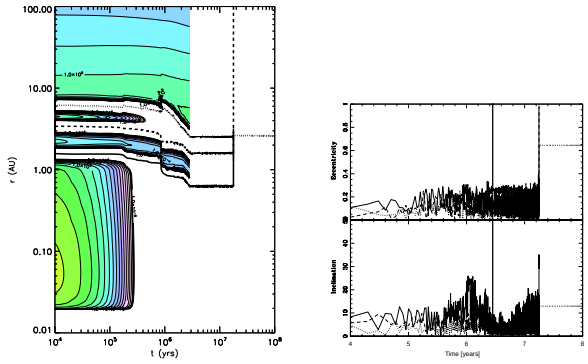

FIG. 7.— Evolution of a three-planet system similar to Fig. 4. Left: Semi-major axis evolution of three planets. Right: Corresponding e and i evolution. Dynamical instability occurs long after the disk dissipation. One planet is ejected, while another one collides with the central star.

planets, both before and after τ_{GD}. All the rates become higher for more massive disks, indicating that stronger convergent/divergent migration in the disk leads to more frequent dynamical instabilities. As in the last subsection, the merger rates are higher for initially small e and i systems (i.e., $d2$ systems).

Fig. 4-8 show some examples of evolution of three-planet systems. Fig. 4 is a dynamically "stable" system, in which there are no ejections, mergers, nor collisions for 100 Myr. Among the survived systems of our "successful" sets, which have the K-S probability of the $a-e$ scattered plots of $P > 0.1$ ($t6d1$, $t7d1$, $t6d1cr$, $t7d1cr$, $t6d2$, $t7d2$, $t7d2cr$, and $t8d2cr$), the fraction of these "stable" cases increases as the initial disk mass decreases, and spans over $\sim 3-19\%$.

Fig. 5 and 6 show the cases where dynamical instability occurs while the gas disk is around. In the former figure, gravitational interactions between planets lead to an ejection of a planet, while in the latter, those lead to a collision with the central star. In these cases, an ejection/collision does not result in a high eccentricity of the remaining planets, probably due to the eccentricity damping in the disk. We find that about 40% of the planetary systems in the successful sets experience either a collision or an ejection *before* the gas disk dissipates.

Fig. 7 and 8 show the cases where dynamical instability occurs long after τ_{GD}. In the former figure, the strong interactions between planets lead to an ejection of one of the planets, and a collision of another planet with the central star. The planet left behind gains a large eccentricity. In the latter figure, such interactions lead to a collision of a planet with the central star, again, leaving the other planets on eccentric, and inclined orbits. About 40% of systems in the successful sets become dynamically unstable *after* the disk dissipation.

The $a-e$ distribution for all the successful sets show the same trend as the representative case in Section 4.1 — the observed $a-e$ distribution is poorly reproduced at τ_{GD}, while at the end of the simulations (100 Myr), the observed distribution is well reproduced. Thus, although the rates of systems which become dynamically unstable are similar before and after τ_{GD}, we find that the eccentricity distribution is largely determined after the disk dissipation, as the previous N-body simulations implicitly assumed.

4.5. *Mass Distribution*

We also studied the $a-M$ and $e-M$ distributions for these sets. We find that the sets with the K-S probability of the $a-e$ scattered plots being $P > 0.1$ also have a high K-S probability for $a-M$ and $e-M$ distributions (see Table 3).

In Fig. 9, we plot a and e against $M_p \sin i$ for a rep-

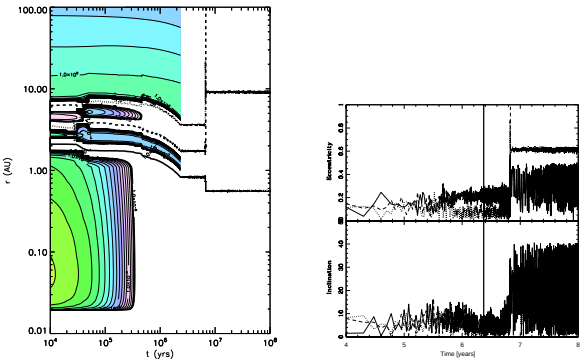

FIG. 8.— Evolution of a three-planet system similar to Fig. 4. Left: Semi-major axis evolution of three planets. Right: Corresponding e and i evolution. Dynamical instability occurs after the disk dissipation. A planet collides with the central star, leaving the other two planets on eccentric, and inclined orbits.

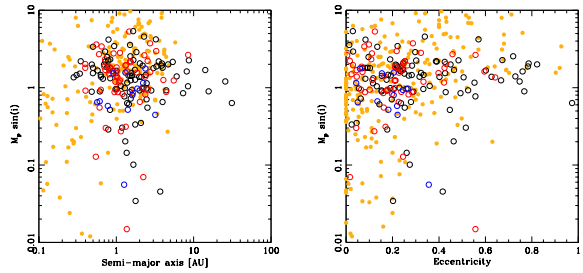

FIG. 9.— Left: Semi-major axis and $M_p \sin i$ scattered plot for $t7d1$. Right: The corresponding eccentricity and $M_p \sin i$ scattered plot. Here, i is chosen randomly over $0 - 180$ deg.

resentative case of $t7d1$. The other cases ($t6d1$, $t6d1cr$, $t7d1cr$, $t6d2$, $t7d2$, $t7d2cr$, and $t8d2cr$) look similar to this. Here, we choose i randomly from $0 - 180$ deg for the simulated planets. These plots mimic the expected $a - M$ and $e - M$ plots, assuming the simulated systems were observed, and the planetary orbits were inclined randomly with respect to the plane of the sky. From these plots, we expect that the future observations will find lower mass planets ($M_p \sin i \lesssim 0.3 M_J$) on large semi-major axis ($\gtrsim 1$ AU).

4.6. *Mean Motion Resonances*

Although it's still too early to derive any statistical trend, some of the extrasolar planetary systems are observed to be in mean motion resonances (MMRs). Thus, it is interesting to investigate whether any of the simulated systems are in such configurations.

At the end of the simulations, our "successful" cases, $t6d1$, $t7d1$, $t6d1cr$, $t7d1cr$, $t6d2$, $t7d2$, $t7d2cr$, and $t8d2cr$ have $\sim 20 - 70$ multi-planet systems. For each of these systems, we estimate whether they are in a particular resonance by using the following resonance variable (Murray & Dermott 1999):

$$\varphi = j_1 \lambda_o + j_2 \lambda_i + j_3 \varpi_o + j_4 \varpi_i \ , \qquad (7)$$

where λ and ϖ are the mean longitude and longitude of pericenter, respectively, and the subscripts i and o indicate inner and outer planets. Here, we focus on near coplanar cases, and thus neglect the terms regarding the longitude of ascending node. When planets are in $p+q : p$ MMR, we can define $(j_1, j_2, j_3, j_4) = (p+q, -p, -q, 0)$, or $(p+q, -p, 0, -q)$.

We follow first- to third-order resonances (2:1, 3:2, 3:1, 5:3, 4:1, 5:2), as well as some higher order resonances (5:1, 7:3, 6:1, 7:2, 7:1, 8:1, 9:2, 9:1, 10:1). In Table 4, we summarize the numbers and kinds of MMRs seen in our systems at the end of the simulations. We find that most of these systems get trapped in MMRs while a gas disk is around, either via migration, or planet–planet scattering. A recent N-body study of three-planet systems (with no gas disk) by Raymond et al. (2008) showed that planet–planet scatterings can populate both low- and high-order MMRs. Our simulations confirm their result, and suggest that the combined effect of disk–planet and planet–planet interactions can generate planets in a variety of MMRs.

In our simulations, most multi-planet systems turn out to be in MMRs ($\sim 70 - 95\%$), while in Raymond et al. (2008), roughly $5 - 10\%$ of dynamically unstable systems ended up being in MMRs. This high rate of planets in MMRs seen in our simulations is clearly inconsistent with the observed systems. Adams et al. (2008) showed that the stochastic forcing effects of turbulence tend to pull planets out of MMRs. If this is the case, the number of planets in MMRs may be much lower.

5. DISCUSSIONS AND CONCLUSIONS

We have studied the evolution of multiple-planet systems in a dissipating gas disk by means of the hybrid code that combines the N-body symplectic integrator SyMBA, and a one-dimensional gas disk evolution code. We simulate disk accretion, gap-opening by planets, and planet migration in a self-consistent manner, and also take account of the effects of eccentricity damping by disk–planet interactions as well as gas accretion by planets. The main goal of this study is to investigate different plausible scenarios and understand how various initial conditions affect the final distributions of observable orbital properties. Specifically, we have investigated the evolution of three-planet systems in a gas disk by utilizing a range of planetary and orbital properties (e.g., M_p, a, e, and i), as well as disk masses, and taking account of the absence/presence of saturation of corotation resonances.

The initial conditions of our planetary systems are motivated by the standard planet formation theory. We assume that giant planets are formed via core accretion, beyond the ice line, on initially nearly circular, and coplanar orbits (see Section 3). Starting with three-planet systems that are initially fully embedded in gas disks, we have shown that the observed $a - e$ distribution can be well reproduced by such models (see Section 4).

It is interesting to further compare the orbital properties of our simulations with current observations. Recently, Wright et al. (2009) pointed out possible differences in distributions of orbital parameters between single- and multiple-planet systems. They found that the highly eccentric orbits ($e > 0.6$) are predominantly associated with apparently single-planet systems. The results of our simulations agree with this, and show that the high eccentricities ($e \gtrsim 0.5 - 0.6$) predominantly occur among single-planet systems at the end of the simulations. This implies that currently observed apparently single-planet systems may have experienced strong dynamical instabilities in the past.

They also pointed out that planets with minimum planetary mass of $> 1\,M_J$ have a broader eccentricity distribution, compared to less massive ones. Although planetary masses in our simulations span only over $0.4-4\,M_J$, we do find a broader eccentricity distribution for planets with $> 1\,M_J$. Such a trend may be naturally explained as a result of strong gravitational interactions between planets, which tend to remove the less massive planet out of the system via an ejection, or a collision, leaving the more massive one on an eccentric orbit.

Another striking difference Wright et al. (2009) pointed out is the difference in semi-major axis distributions for single- and multiple-planet systems. The a distribution of single-planet systems is characterized by the so-called 3-day peak and the jump in planetary abundance beyond 1 AU, while the corresponding distribution for multiple-planet systems is rather uniform. Such a difference may be well-explained if the evolution of single-planet systems has been dominated by planet–planet scatterings as opposed to planet migration, while that of multiple-planet systems has been dominated by planet migration. Although we do not see such a difference in orbital distributions between single- and multiple-planet systems in our simulations, this may be partly because we don't have good numerical resolutions for $< 0.2\,$AU. Interestingly, we find a group of planets with a range of e that are located around 0.1 AU just before they are ejected out of the systems, or collides with the central star. Although our code does not include the tidal evolution directly, the separate calculations of tidal evolution of these systems indicate that they could be candidates of observed close-in, tidally-affected planets. Nagasawa et al. (2008) pointed out that such close-in planets can be formed even without migration in gas disks. They studied the orbital evolution of three-planet systems with Jupiter mass by including the tidal circularization, and showed that Kozai mechanism combined with tidal orbital circularization (i.e., Kozai migration) can form these close-in planets for $\sim 30\%$ cases of their simulations.

Recent observations of Rossiter-McLaughlin effects started revealing an interesting subset of close-in exoplanets which have clearly misaligned orbits, or even retrograde ones (e.g., Winn et al. 2009; Narita et al. 2009). Out of at least 17 transiting systems with the observed projected stellar obliquity, 8 have a clearly misaligned orbit ($> 10\,$deg), among which 3 are on retrograde orbits. We find that, from both simulations of three-planet systems with and without gas disks, the fractions of clearly inclined planets are$\sim 15\%$ and $\sim 65\%$, respectively, while the rate of planets on retrograde orbits is less than 1% for both types of simulations. Thus, our results indicate that mechanisms other than planet–planet scatterings may be responsible for the observed high rate of close-in, retrograde planets. Note, however, Nagasawa et al. (2008) showed that inclinations could be more broadly distributed if close-in planets are formed via Kozai migration. If this is the case, the inclination distribution of close-in planets may be significantly different from that of planets on further orbits.

Our investigations are affected by several significant uncertainties.

First of all, the initial conditions for this kind of simulations are highly uncertain. For example, we assume that nearly fully-grown giant planets are initially embedded in a gas disk. In reality, however, planets would start opening gaps as they grow, and therefore they should not be fully embedded in a gas disk initially. However, the planets in our simulations open gaps in a time on the order of the orbital periods (i.e. less than several tens of years), which are shorter than, or at most comparable to, both the dynamical, and migration timescales. Therefore, we don't expect a huge difference in the outcome due to this approximation.

Also, our choice of the initial planetary properties like mass, and semimajor axis, although motivated by the core accretion scenario, is rather arbitrary. To better approximate the initial conditions, we could have performed planet formation simulations as in Thommes et al. (2008). However, such simulations are computationally very expensive for executing statistical studies.

Secondly, planet migration in our models do not take account of the effects of corotation resonances. Since corotation torques are sensitive to sharp gradients in the surface mass density, they may have a significant effect on some of the planets simulated here, which are massive enough to open a gap in the disk, but not massive enough to open a clean gap and saturate corotation resonances. The so-called Type III migration due to the corotation torques tend to accelerate the inward planet migration (Masset & Papaloizou 2003), and thus we are likely to underestimate planet migration rates for intermediate-mass (Saturn-like) planets, which do not open a clean gap.

Regarding eccentricity evolution, we focus on the effects of first-order resonances. Although this is a fair approximation for planets with small eccentricities (Goldreich & Tremaine 1980), higher-order resonances may become important if e is excited to a large value in the disk. Taking account of higher-order resonances, Moorhead & Adams (2008) semi-analytically showed that the eccentricity evolution timescales are decreased by a factor of a few, but the overall trend of eccentricity evolution (e.g., damping or driving of e) does not change. Furthermore, they suggested that eccentricity decreases for $0.1 \lesssim e \lesssim 0.5$ as long as corotation resonances are unsaturated, while eccentricity can rapidly increase when corotation resonances are fully saturated. On the other hand, current hydro simulations show that disk-planet interactions excite eccentricity upto ~ 0.2 (e.g. D'Angelo et al. 2006). As already mentioned, our simulations don't take account of eccentricity excitation effect due to disk–planet interactions. Thus, our simulations may underestimate the eccentricity excitation rate for massive planets, which open a clean gap, and have a sufficient eccentricity to saturate corotation resonances. Clearly, this is an issue which requires a further investigation.

Finally, our gas disk is removed exponentially once the randomly selected disk dissipation time is reached. Although such a disk removal is included to mimic the effect of photoevaporation, we did not model its physics directly. This is because the photoevaporation rate is difficult to estimate accurately, due to its sensitivity to the stellar flux, which in turn depends on the disk accretion rate, as well as the stellar environment (Matsuyama et al. 2003).

Bearing these in mind, our simulations successfully reproduced the general trends of the observed properties, starting with the initial conditions expected from core accretion scenario. We summarize our findings below.

1. Although the occurrence of dynamical instabilities before and after the disk dissipation is comparable, the e distribution is largely determined by planet–planet interactions after τ_{GD}.

2. The a distribution is largely determined by disk–planet interactions. To explain the current a distribution, a disk mass has to be comparable to, or larger than, a planetary mass.

3. There may be an optimum disk mass to reproduce the observed $a - e$ distribution.

4. Dynamical instabilities in a gas disk which involve ejections/collisions/mergers tend not to lead to large eccentricities of remaining planets.

5. Initially nearly coplanar systems tend to have a higher merger rate between planets.

6. For the range of disk masses we use, we do not see a significant difference in outcomes by taking account of the saturation of corotation resonances, and hence the reduction of e damping.

7. We find that the combined effects of disk–planet and planet–planet interactions lead to both low- and high-order MMRs. Our results also indicate that, without perturbing effects (e.g., turbulence), too many planets may be trapped in MMRs.

8. Starting with relatively well-aligned, prograde orbits, we find that planet–planet interactions are not efficient in producing the planets on retrograde orbits.

This work was supported by NSF Grant AST-0507727 (to F. A. R.) and by a Spitzer Theory grant, as well as a grant from Natural Sciences and Engineering Research Council of Canada (to E. W. T.). We thank an anonymous referee for careful reading, and helpful suggestions, which have improved this paper significantly. S. M. extends a sincere thank you to Ralph Pudritz for making SHARCNET available for many of the simulations shown in this work.

REFERENCES

Adams, F. C. & Laughlin, G. 2003, Icarus, 163, 290
Adams, F. C., Laughlin, G., & Bloch, A. M. 2008, ApJ, 683, 1117
Alexander, R. D., Clarke, C. J., & Pringle, J. E. 2006, MNRAS, 369, 229
Artymowicz, P. 1993, ApJ, 419, 155
Bryden, G., Lin, D. N. C., & Ida, S. 2000, ApJ, 544, 481
Chatterjee, S., Ford, E. B., Matsumura, S., & Rasio, F. A. 2008, ApJ, 686, 580
Chiang, E. I., Fischer, D., & Thommes, E. 2002, ApJL, 564, L105
Currie, T., Lada, C. J., Plavchan, P., Robitaille, T. P., Irwin, J., & Kenyon, S. J. 2009, ApJ, 698, 1
D'Angelo, G., Kley, W., & Henning, T. 2003, ApJ, 586, 540
D'Angelo, G., Lubow, S. H., & Bate, M. R. 2006, ApJ, 652, 1698
Duncan, M. J., Levison, H. F., & Lee, M. H. 1998, AJ, 116, 2067
Ford, E. B., Havlickova, M., & Rasio, F. A. 2001, Icarus, 150, 303
Ford, E. B. & Rasio, F. A. 2008, ApJ, 686, 621
Goldreich, P. & Sari, R. 2003, ApJ, 585, 1024
Goldreich, P. & Tremaine, S. 1980, ApJ, 241, 425
Hillenbrand, L. A. 2005, review article in "A Decade of Discovery", astro-ph/0511083
Ivanov, P. B., Papaloizou, J. C. B., & Polnarev, A. G. 1999, MNRAS, 307, 79
Jurić, M. & Tremaine, S. 2008, ApJ, 686, 603
Kokubo, E. & Ida, S. 2002, ApJ, 581, 666
Kominami, J. & Ida, S. 2004, Icarus, 167, 231
Lee, M. H. & Peale, S. J. 2002, ApJ, 567, 596
Lewis, J. S. 1974, Science, 186, 440
Lin, D. N. C. & Papaloizou, J. 1986, ApJ, 307, 395
Lodders, K. 2004, ApJ, 611, 587
Masset, F. S. & Papaloizou, J. C. B. 2003, ApJ, 588, 494
Matsuyama, I., Johnstone, D., & Hartmann, L. 2003, ApJ, 582, 893
Menou, K. & Goodman, J. 2004, ApJ, 606, 520
Moorhead, A. V. & Adams, F. C. 2005, Icarus, 178, 517
—. 2008, Icarus, 193, 475
Murray, C. D. & Dermott, S. F. 1999, Solar system dynamics (Solar system dynamics by Murray, C. D., 1999)
Nagasawa, M., Ida, S., & Bessho, T. 2008, ApJ, 678, 498
Narita, N., Sato, B., Hirano, T., & Tamura, M. 2009, PASJ, 61, L35
Ogilvie, G. I. & Lubow, S. H. 2002, MNRAS, 330, 950
Rasio, F. A., Tout, C. A., Lubow, S. H., & Livio, M. 1996, ApJ, 470, 1187
Raymond, S. N., Barnes, R., Armitage, P. J., & Gorelick, N. 2008, ApJL, 687, L107
Shakura, N. I. & Sunyaev, R. A. 1973, A&A, 24, 337
Sicilia-Aguilar, A., Hartmann, L. W., Fürész, G., Henning, T., Dullemond, C., & Brandner, W. 2006, AJ, 132, 2135
Simon, M. & Prato, L. 1995, ApJ, 450, 824
Snellgrove, M. D., Papaloizou, J. C. B., & Nelson, R. P. 2001, A&A, 374, 1092
Tanigawa, T. & Watanabe, S.-i. 2002, ApJ, 580, 506
Thommes, E. W. 2005, ApJ, 626, 1033
Thommes, E. W., Matsumura, S., & Rasio, F. A. 2008, Science, 321, 814
Ward, W. R. 1997, Icarus, 126, 261
Weidenschilling, S. J. & Marzari, F. 1996, Nature, 384, 619
Winn, J. N., Johnson, J. A., Fabrycky, D., Howard, A. W., Marcy, G. W., Narita, N., Crossfield, I. J., Suto, Y., Turner, E. L., Esquerdo, G., & Holman, M. J. 2009, ApJ, 700, 302
Wisdom, J. & Holman, M. 1991, AJ, 102, 1528
Wittenmyer, R. A., Endl, M., & Cochran, W. D. 2007, ApJ, 654, 625
Wright, J. T., Marcy, G. W., Fischer, D. A., Butler, R. P., Vogt, S. S., Tinney, C. G., Jones, H. R. A., Carter, B. D., Johnson, J. A., McCarthy, C., & Apps, K. 2007, ApJ, 657, 533
Wright, J. T., Upadhyay, S., Marcy, G. W., Fischer, D. A., Ford, E. B., & Johnson, J. A. 2009, ApJ, 693, 1084

TABLE 2
Ejected, Collided, and Merged Planets

	Ejections			Collisions			Mergers		
Set No.	Before τ_{GD}	After τ_{GD}	Total	Before τ_{GD}	After τ_{GD}	Total	Before τ_{GD}	After τ_{GD}	Total
t5d1	110 (36.7)	11 (23.4)	121	21 (7)	9 (19.1)	30	58 (19.3)	2 (4.26)	60
t6d1	62 (20.7)	35 (23.6)	97	6 (2)	11 (7.43)	17	42 (14)	7 (4.73)	49
t7d1	45 (15.3)	46 (21.6)	91	1 (0.333)	9 (4.23)	10	25 (8.33)	8 (3.76)	33
t8d1	35 (11.7)	29 (13.6)	64	0 (0)	7 (3.27)	7	15 (5)	2 (0.935)	17
t9d1	25 (8.33)	26 (10.2)	51	0 (0)	9 (3.53)	9	12 (4)	3 (1.18)	15
t5d1cr	118 (39.3)	16 (29.6)	134	18 (6)	3 (5.56)	21	54 (18)	4 (7.41)	58
t6d1cr	83 (27.7)	31 (27.9)	114	11 (3.67)	14 (12.6)	25	41 (13.7)	8 (7.21)	49
t7d1cr	39 (13)	46 (20.8)	85	1 (0.333)	10 (4.52)	11	19 (6.33)	9 (4.07)	28
t8d1cr	47 (15.7)	27 (12.1)	74	0 (0)	2 (0.893)	2	14 (4.67)	3 (1.34)	17
t9d1cr	31 (10.3)	36 (14.5)	67	1 (0.333)	2 (0.806)	3	11 (3.67)	3 (1.21)	14
t5d2	99 (33)	14 (30.4)	113	19 (6.33)	3 (6.52)	22	87 (29)	3 (6.52)	90
t6d2	61 (20.3)	31 (23.5)	92	8 (2.67)	5 (3.79)	13	61 (20.3)	3 (2.27)	64
t7d2	45 (15.3)	29 (16.2)	74	4 (1.33)	5 (2.79)	9	44 (14.7)	7 (3.91)	51
t8d2	33 (11)	19 (8.88)	52	2 (0.667)	5 (2.34)	7	37 (12.3)	4 (1.87)	41
t9d2	25 (8.33)	36 (16)	61	0 (0)	2 (0.889)	2	41 (13.7)	6 (2.67)	47
t5d2cr	95 (31.7)	12 (33.3)	107	18 (6)	1 (2.78)	19	89 (29.7)	1 (2.78)	90
t6d2cr	53 (17.7)	33 (23.6)	86	11 (3.67)	8 (5.71)	21	62 (20.7)	4 (2.86)	66
t7d2cr	41 (13.7)	30 (17.4)	71	5 (1.67)	2 (1.16)	7	52 (17.3)	6 (3.49)	58
t8d2cr	28 (9.33)	20 (10.1)	48	3 (1)	3 (1.51)	6	51 (17)	4 (2.01)	55
t9d2cr	27 (9)	17 (7.83)	44	0 (0)	4 (1.84)	4	43 (14.3)	2 (0.922)	45

Note. — Numbers of planets which are ejected from the system, collided with the central star, and merged with another planet, before and after the gas dissipation time τ_{GD}, as well as throughout the simulations. Larger number of collisions before τ_{GD} indicates more efficient planet migration, while the larger number of ejections indicates higher occurrences of dynamical instability. The percentages of planets in more than two-planet systems which are ejected/collided/merged are shown inside the brackets.

TABLE 3 The 2D K-S test for a, e, and M_p distributions

Set No.		τ_{GD} and τ_{fin} D	τ_{GD} and τ_{fin} P	τ_{GD} and Obs D	τ_{GD} and Obs P	τ_{fin} and Obs D	τ_{fin} and Obs P
t5d1	a vs e	$1.20e-2$	1.000	$6.95e-2$	$5.55e-2$	$7.80e-2$	$1.94e-2$
t5d1	m vs e	$1.20e-2$	1.000	$6.70e-2$	$5.75e-2$	$7.80e-2$	$1.71e-2$
t5d1	m vs a	$1.20e-2$	0.9999	$6.85e-2$	$5.19e-2$	$7.80e-2$	$1.92e-2$
t6d1	a vs e	0.197	0	0.190	0	$3.20e-2$	0.842
t6d1	m vs e	0.197	0	0.216	0	$4.40e-2$	0.440
t6d1	m vs a	0.197	0	0.209	0	$4.15e-2$	0.528
t7d1	a vs e	0.281	0	0.314	0	$3.70e-2$	0.693
t7d1	m vs e	0.281	0	0.325	0	$5.65e-2$	0.172
t7d1	m vs a	0.281	0	0.328	0	$5.40e-2$	0.212
t8d1	a vs e	0.272	0	0.327	0	$7.30e-2$	$4.03e-2$
t8d1	m vs e	0.272	0	0.341	0	$7.90e-2$	$1.60e-2$
t8d1	m vs a	0.271	0	0.332	0	$7.35e-2$	$3.12e-2$
t9d1	a vs e	0.293	0	0.392	0	0.110	0
t9d1	m vs e	0.293	0	0.395	0	0.112	0
t9d1	m vs a	0.293	0	0.395	0	0.109	0
t5d1cr	a vs e	$2.00e-2$	0.998	$5.75e-2$	0.175	$7.15e-2$	$4.29e-2$
t5d1cr	m vs e	$1.85e-2$	0.999	$5.75e-2$	0.146	$7.10e-2$	$3.83e-2$
t5d1cr	m vs a	$1.85e-2$	0.9995	$5.60e-2$	0.180	$7.10e-2$	$4.54e-2$
t6d1cr	a vs e	0.164	0	0.125	0	$5.35e-2$	0.238
t6d1cr	m vs e	0.164	0	0.147	0	$5.05e-2$	0.278
t6d1cr	m vs a	0.164	0	0.154	0	$5.10e-2$	0.281
t7d1cr	a vs e	0.299	0	0.334	0	$5.20e-2$	0.269
t7d1cr	m vs e	0.299	0	0.346	0	$6.60e-2$	$6.96e-2$
t7d1cr	m vs a	0.298	0	0.350	0	$5.90e-2$	0.138
t8d1cr	a vs e	0.275	0	0.336	0	$7.40e-2$	$3.67e-2$
t8d1cr	m vs e	0.276	0	0.341	0	$8.30e-2$	$1.01e-2$
t8d1cr	m vs a	0.275	0	0.350	0	$8.35e-2$	0
t9d1cr	a vs e	0.290	0	0.376	0	$9.70e-2$	0
t9d1cr	m vs e	0.288	0	0.381	0	0.101	0
t9d1cr	m vs a	0.288	0	0.381	0	0.101	0
t5d2	a vs e	$1.65e-2$	0.9999	$6.60e-2$	$8.45e-2$	$8.10e-2$	$1.64e-2$
t5d2	m vs e	$1.55e-2$	0.9999	$6.55e-2$	$6.80e-2$	$8.05e-2$	$1.22e-2$
t5d2	m vs a	$1.60e-2$	0.9999	$6.55e-2$	$7.51e-2$	$8.05e-2$	$1.41e-2$
t6d2	a vs e	0.173	0	0.157	0	$4.10e-2$	0.541
t6d2	m vs e	0.172	0	0.177	0	$5.25e-2$	0.236
t6d2	m vs a	0.173	0	0.178	0	$4.80e-2$	0.344
t7d2	a vs e	0.221	0	0.242	0	$3.85e-2$	0.643
t7d2	m vs e	0.220	0	0.260	0	$5.30e-2$	0.225
t7d2	m vs a	0.221	0	0.261	0	$4.90e-2$	0.313
t8d2	a vs e	0.245	0	0.314	0	$8.25e-2$	$1.29e-2$
t8d2	m vs e	0.244	0	0.324	0	$9.60e-2$	0
t8d2	m vs a	0.245	0	0.323	0	$8.60e-2$	0
t9d2	a vs e	0.277	0	0.324	0	$6.95e-2$	$5.63e-2$
t9d2	m vs e	0.277	0	0.329	0	$7.05e-2$	$4.46e-2$
t9d2	m vs a	0.277	0	0.337	0	$7.60e-2$	$2.27e-2$
t5d2cr	a vs e	$1.35e-2$	0.9999	$7.70e-2$	$2.62e-2$	$8.70e-2$	0
t5d2cr	m vs e	$1.20e-2$	0.9999	$7.65e-2$	$1.92e-2$	$8.70e-2$	0
t5d2cr	m vs a	$1.15e-2$	0.9999	$7.60e-2$	$2.32e-2$	$8.70e-2$	0
t6d2cr	a vs e	0.227	0	0.153	0	$9.20e-2$	0
t6d2cr	m vs e	0.227	0	0.175	0	$9.25e-2$	0
t6d2cr	m vs a	0.227	0	0.168	0	$9.20e-2$	0
t7d2cr	a vs e	0.215	0	0.224	0	$2.90e-2$	0.915
t7d2cr	m vs e	0.214	0	0.242	0	$4.80e-2$	0.330
t7d2cr	m vs a	0.214	0	0.239	0	$4.05e-2$	0.554
t8d2cr	a vs e	0.229	0	0.263	0	$5.35e-2$	0.242
t8d2cr	m vs e	0.229	0	0.271	0	$6.15e-2$	0.108
t8d2cr	m vs a	0.228	0	0.276	0	$6.10e-2$	0.112

TABLE 4
Numbers of Planetary Systems in MMRs

Set No.	2 : 1	3 : 2	3 : 1	4 : 1	5 : 2	5 : 1	6 : 1	7 : 2	7 : 1	8 : 1	9 : 2	9 : 1	10 : 1
t6d1	6	0	16	5	4	1	2	2	0	0	0	0	0
t7d1	23	1	22	7	5	1	1	1	1	1	0	0	0
t6d1cr	5	0	6	5	2	0	0	1	0	1	0	0	0
t7d1cr	23	0	17	7	7	3	5	2	2	0	0	0	1
t6d2	10	0	17	7	4	0	1	0	0	0	0	0	0
t7d2	14	2	19	11	6	0	2	1	1	1	1	0	1
t7d2cr	14	2	19	11	6	0	2	1	1	1	1	0	1
t8d2cr	21	0	28	7	13	6	4	2	0	0	0	1	0

Note. — The numbers of systems which have each kind of MMRs. The shown sets are successful cases which have $P > 0.1$ for the K-S test of the observed and simulated $a - e$ scattered plot. Most of these planets are trapped in MMRs while a gas disk is around.

Table 3 – Continued

Set No.		τ_{GD} and τ_{fin} D	P	τ_{GD} and Obs D	P	τ_{fin} and Obs D	P
t9d2cr	a vs e	0.236	0	0.300	0	$7.85e-2$	$2.20e-2$
t9d2cr	m vs e	0.236	0	0.304	0	$8.30e-2$	$1.00e-2$
t9d2cr	m vs a	0.236	0	0.310	0	$8.35e-2$	0

Note. — The results of the 2D K-S test for the combinations of semimajor axis, eccentricity, and planetary masses. We compare the simulated results at $\tau_{fin} = 100\,\mathrm{Myr}$ with the observed planets between 0.2 AU $\lesssim a \lesssim$ 6 AU, and $0.3M_J \lesssim M_p \lesssim 4M_J$. The K-S statistic D, and the corresponding probability P are shown for each comparison. We reject the null hypothesis for P less than 0.1. Here, the null hypothesis is that the pair of samples used in the test is drawn from the same distribution.